Fermi Surface Topology and the Superconducting Gap Function in UPd_2Al_3: A Neutron Spin-Echo Study

E. Blackburn,[1,2,*] A. Hiess,[1] N. Bernhoeft,[3] M. C. Rheinstädter,[1] W. Häußler,[1,4] and G. H. Lander[2]

[1]*Institut Laue-Langevin, Boîte Postale 156, F-38042 Grenoble, France*

[2]*European Commission, JRC, Institute for Transuranium Elements, Postfach 2340, D-76125 Karlsruhe, Germany*

[3]*Département de Recherche Fondamentale sur la Matière Condensée, CEA-Grenoble, F-38054 Grenoble, France*

[4]*FRM-II, Technische Universität München, Lichtenbergstrasse 1, D-85748 Garching, Germany*

(Received 11 April 2006; published 1 August 2006)

We report on a single crystal neutron spin-echo investigation of the low-energy dynamic response in the heavy-fermion superconductor UPd_2Al_3 in the vicinity of the antiferromagnetic wave vector $\mathbf{Q}_0 = (0\ 0\ 0.5)$. Well inside the superconducting phase, antiferromagnetic quasielastic scattering, which is present in the normal state, is absent for relaxation times up to 10 ns, equivalent to an energy resolution of $\sim 1\ \mu$eV. This places strong constraints on possible models for this magnetic superconductor.

DOI: 10.1103/PhysRevLett.97.057002 PACS numbers: 74.70.Tx, 71.27.+a, 76.60.Lz, 78.70.Nx

UPd_2Al_3 is an example of the rare coexistence of antiferromagnetic order and superconductivity where both phenomena appear to be generated by the same electronic states [1,2]. With transition temperatures $T_N = 14.3$ K and $T_{sc} = 1.8$ K at ambient pressure, it is one of the few examples amenable to neutron inelastic scattering studies. The interplay of the magnetism and the superconductivity is a matter of lively debate, and several authors have posited that the superconductivity is unconventional and may be magnetically mediated [3–5].

To understand the superconductivity, a detailed knowledge of both the symmetry and magnitude of the gap function and its relationship with the Fermi-surface topology is crucial. The most direct information is usually accessed through the quasiparticle *charge* spectral function as studied through tunneling spectroscopy. In the case of UPd_2Al_3, the strongly enhanced *magnetic* susceptibility (on the scale of $k_B T_{sc}$) means that the unique advantages of neutron inelastic scattering (namely, simultaneous microscopic wave vector and subthermal energy resolution) can be used to investigate both the translational symmetry and the magnitude of the gap function.

Previous neutron three-axis spectroscopy (TAS) investigations of UPd_2Al_3 [6,7] have shown that the low-energy dynamic response at the antiferromagnetic zone center, $\mathbf{Q}_0 = (0\ 0\ 0.5)$, differs in the superconducting and normal states. In the superconducting state two inelastic contributions to the magnetic response are observed close to $\mathbf{Q}_0$ at energy transfers of $\Delta E = 0.35$ and 1.4 meV. The signal at lower energy transfer apparently corresponds to excitations across the superconducting energy gap [7] and disappears for $T > T_{sc}$ and on applying a magnetic field $B > B_{c2}$ [8]. The 1.4 meV response is broad and dispersive. In the normal state, a strong, and within the available energy resolution (± 0.1 meV), quasielastic response localized at $\mathbf{Q}_0$ coexists with the 1.4 meV inelastic signal. For $T_{sc} < T < 7$ K the extent of the low-energy scattering declines with $k_B T$ [7], suggesting the existence of quasielastic scattering characterized by a constant bare energy linewidth. Because of the decrease in thermal population, below T_{sc} this low-energy signal can no longer be resolved in the presence of the magnetic Bragg peak on current cold neutron three-axis spectrometers. The presence, or otherwise, of quasielastic scattering is important in evaluating the nature of the superconducting state. In order to clarify the experimental situation the present study uses the neutron spin-echo (NSE) technique [9], which, while rarely applied to magnetic studies in single crystals, offers an increase of ~ 2 orders of magnitude in energy resolution over the TAS measurements.

In spin echo, the neutron time of flight is encoded in the precession of the neutron spin. The polarized incident beam passes through a magnetic field B_1, perpendicular to the neutron polarization, acquiring a precession angle $\phi_1 = \gamma l_1 B_1 / v_1$ over the distance l_1 to the sample, where γ is the neutron gyromagnetic ratio and v_1 the neutron velocity. The incident beam has a large velocity spread (typically $\pm 8\%$), so there is no overall polarization at the sample.

The scattered neutron beam passes through a second arm, acquiring a precession angle $\phi_2 = \gamma l_2 B_2 / v_2$. This precession occurs in the reverse sense for neutrons that have experienced a π spin flip, which may be induced by spin-dependent scattering, giving a total precession angle $\Delta\phi = \phi_1 - \phi_2$. For elastic scattering $v_1 = v_2$, and so if $l_1 B_1 = l_2 B_2$, $\Delta\phi = 0$ for all incoming neutron velocities. If $\Delta\phi$ is altered, for example, by ramping the relative magnetic precession field for the incident and scattered beams, a series of oscillations called an *echo group* is observed at the detector. The beam polarization is taken to be the maximal value of this echo group, and is therefore $P_{\mathrm{NSE}} \sim P_s |\langle \exp(i\Delta\phi) \rangle|$, where P_s is the modulus of the beam polarization just after scattering.

In an inelastic scattering event ($v_2 \neq v_1$), there is a phase shift $\Delta\phi = \omega t$ for small changes in the neutron velocity, where $\hbar\omega$ is the energy transfer between neutron and sample. $P_{\mathrm{NSE}}(t)$ therefore encodes information on the scattering function for a particular Fourier (decorrelation)

time t:

$$P_{\mathrm{NSE}}(t) = P_s \left| \frac{\int S(\mathbf{Q}, \omega) e^{i\omega t} d\omega}{\int S(\mathbf{Q}, \omega) d\omega} \right|; \qquad (1)$$

i.e., $P_{\mathrm{NSE}}(t)$ is proportional to the normalized intermediate scattering function $S(\mathbf{Q}, t)/S(\mathbf{Q}, 0)$. For a quasielastic response assumed to have a Lorentzian line shape,

$$S(\mathbf{Q}, \omega) \propto \frac{\Gamma}{(\Gamma^2 + \omega^2)} \frac{\omega}{1 - \exp(-\hbar\omega/k_B T)}. \qquad (2)$$

In the high-temperature limit $k_B T \gg \hbar\omega$, $P_{\mathrm{NSE}} \propto e^{-\Gamma t}$, where Γ is the autocorrelation decay rate. For lower temperatures the simple time exponential relation no longer holds, and P_{NSE} has to be calculated numerically (for further discussion of this point, see Ref. [10]).

UPd_2Al_3 has a hexagonal chemical unit cell, with lattice parameters $a = b = 5.35$ Å, $c = 4.185$ Å at room temperature. In the ordered state, neutron diffraction observes a magnetic polarization of $0.85\mu_B$ pointing along the basal plane crystal axes [11]. These ferromagnetic basal planes are stacked antiferromagnetically along the c axis, giving the ordered magnetic propagation wave vector $\mathbf{Q}_0 = (0\ 0\ 0.5)$. The moments are generated by the $5f$ shell of the uranium ions [12].

The single crystal from Ref. [7], with a nominal composition of $UPd_{2.02}Al_{3.03}$ from the components prior to growth and a mass of ~2.7 g, was aligned to give an a^*-c^* scattering plane, with the b axis vertical and mounted on the neutron spin-echo spectrometer IN11A at the Institut Laue-Langevin, Grenoble. The incident wavelength was set to 5.5 Å using a velocity selector with a ±8% spread. A 2D detector covering an angular range of $0.9° \times 0.9°$ was used. The first magnetic zone center at (0 0 0.5) was selected for study, to maximize the magnetic signal and because a low 2θ angle reduces the overlap of the magnetic fields in the two arms of the spectrometer. The use of a single crystal and the angular acceptance of the detector limits the range of scattered velocities. Using the lattice parameter measured independently for this sample at 50 mK, the wavelength selected by the crystal was found to be 5.52 ± 0.08 Å at (0 0 0.5).

Figure 1(a) shows the neutron scattering intensity observed in a rocking scan about the magnetic peak at $\mathbf{Q}_0$ at a constant scattering angle. To reduce the amount of Bragg scattering an angular position 1.5° away from the Bragg peak [the vertical arrow in Fig. 1(a)] was selected to look for quasielastic scattering. This sample orientation corresponds to $\mathbf{Q}' = (0.015\ 0\ 0.5)$ at the nominal wavelength. From the previous TAS work, this position is sufficiently close to the magnetic zone center to see a clear quasielastic signal at $T = 2$ K [6,7], especially as the instrumental momentum resolution is relaxed in respect to that observed for the Bragg peak because of the available wavelength spread.

Echo groups were measured at a selection of Fourier times, at both the Bragg peak [Fig. 1(b)] with 5 s per point and $\mathbf{Q}'$ [Fig. 1(c)] with 15 min per point. In all cases the echo groups were fitted using sine waves. The number of points per period was selected by choosing the magnetic field step length. By measuring more than one period, the existence of an echo and a reliable estimate of the amplitude was ensured [10,13].

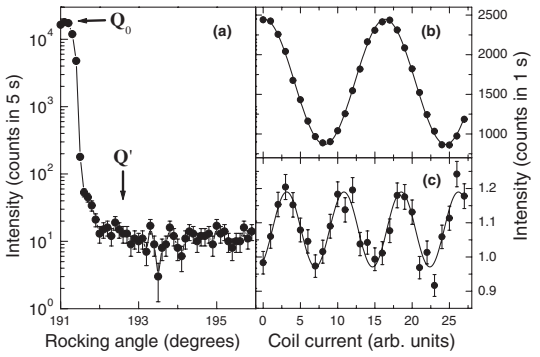

FIG. 1. (a) Intensity observed on rotating the sample in the scattering plane at a fixed scattering angle 2θ corresponding to the (0 0 0.5) magnetic Bragg peak at $T = 50$ mK. The arrows indicate the positions of the echo groups measured as a function of coil current at (b) $\mathbf{Q}_0 = (0\ 0\ 0.5)$, $t = 0.49$ ns with 5 s per point, and (c) $\mathbf{Q}' = (0.015\ 0\ 0.5)$, $t = 7.7$ ns with 15 min per point (intensities normalized to counts per second). The abscissa values of the coil current were chosen to illustrate different numbers of periods in the two cases.

At the Bragg peak $\mathbf{Q}_0$, echo groups were measured at 52 Fourier times, giving an amplitude $I(\mathbf{Q}_0, t)$ [Fig. 2(a)]. This was normalized using xyz polarization to estimate $I(\mathbf{Q}_0, 0) = \int I(\mathbf{Q}_0, \omega) d\omega$. Assuming that the signal $I(\mathbf{Q}_0, t)/I(\mathbf{Q}_0, 0)$ at $T = 50$ mK is generated by a *static* Bragg peak $[S(\mathbf{Q}_0, t)/S(\mathbf{Q}_0, 0) = 1]$, the observed deviations from 1 are assigned to instrumental resolution effects. This is the best estimate available of the spectrometer resolution at low energy and momentum transfers for scattering close to $\mathbf{Q}_0$.

At $\mathbf{Q}'$ a selection of Fourier times was examined in the superconducting state at 50 mK, in the antiferromagnetic state at 2 K, and in the paramagnetic state at 15 K [Fig. 2(b)]. The data are normalized to $S(\mathbf{Q}', 0)$ and corrected for resolution.

First observations are that the scattering function clearly relaxes with t at 2 and 15 K. At 15 K, there is ~8 times more dynamic scattering than at 2 K. In the superconducting ordered state at 50 mK, the data suggest a constant ratio $S(\mathbf{Q}', t)/S(\mathbf{Q}', 0) = 1$, indicating that the scattering is purely static over the measured time window.

To analyze $S(\mathbf{Q}', t)$ more quantitatively as a function of Fourier time t we suppose that at all temperatures there is a superposition of a quasielastic (relaxing) signal with a static t-independent component (resulting from the tail of the Bragg peak and/or instrumental background). In the simplest approach, which is valid for $\hbar\omega \ll k_B T$, the quasielastic scattering is modeled as an exponential response, and so the data at $\mathbf{Q}'$ are fitted using

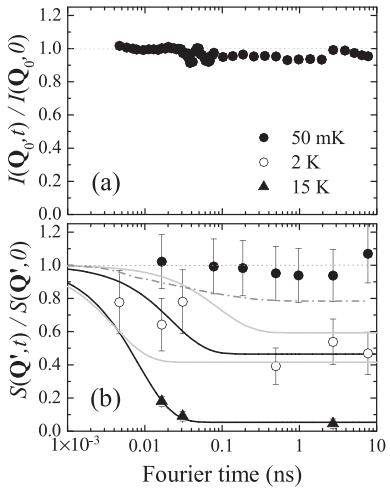

FIG. 2. (a) Momentum and time-dependent intermediate scattering function $I(\mathbf{Q}_0, t)$ normalized to $I(\mathbf{Q}_0, 0)$ as a function of Fourier time at 50 mK (solid circles). (b) Momentum and time-dependent intermediate scattering function $S(\mathbf{Q}', t)$ normalized to $S(\mathbf{Q}', 0)$ and corrected for resolution using the measurements in panel (a) as a function of Fourier time at 50 mK (solid circles), 2 K (open circles), and 15 K (solid triangles). The dotted lines mark $I(\mathbf{Q}, t)/I(\mathbf{Q}, 0) = 1$ and $S(\mathbf{Q}', t)/S(\mathbf{Q}', 0) = 1$. The black lines are simple exponential fits described in the text and summarized in Table I. The gray lines are possible extremal decay curves at 2 K, illustrating the uncertainty at this temperature. The dash-dotted gray line is a numerical calculation of the predicted scattering at 50 mK assuming a quasielastic response with $\Gamma = 0.03$ meV.

$$S(\mathbf{Q}', t)/S(\mathbf{Q}', 0) = y_0 + (1 - y_0)\exp(-\Gamma t), \qquad (3)$$

where y_0 is time independent. The energy integration of $S(\mathbf{Q}', 0)$ includes the major part of the quasielastic signal at each temperature. The fitted values are given in Table I. We note that it is only at 15 K that this exponential form can be easily related to the (Lorentzian) linewidth of the quasielastic scattering as observed by TAS. Nevertheless, this provides a measure of the magnitude of the dynamics at 2 K. The widths Γ obtained in the fits are the same order of magnitude as the values derived by Bernhoeft *et al.* [7] from TAS data. Considering the model dependencies and simplifications assumed in both the TAS and spin-echo data, this is reasonable. The gray lines in Fig. 2(b) mark the decay curves corresponding to the extremal error values at 2 K.

The data taken at 50 mK are clearly in the low temperature regime and should be analyzed accordingly. However, no dynamic contribution is visible in the data. Numerical simulation [10] of Eq. (1) including a fixed static component indicates that Γ must be significantly less than 0.03 meV at $\mathbf{Q}'$ [dash-dotted gray line in Fig. 2(b)]. Any inelastic mode would require an energy gap substantially greater than this for the decay to be washed out by the oscillations, and would then have been observed by TAS.

TABLE I. Γ, $S(\mathbf{Q}', 0)$, $1 - y_0$, and $y_0 S(\mathbf{Q}', 0)$, obtained as described in the text.

	Γ (meV)	$S(\mathbf{Q}', 0)$ (counts $\cdot$ s^{-1})	$1 - y_0$	$y_0 S(\mathbf{Q}', 0)$ (counts $\cdot$ s^{-1})
50 mK		0.11 ± 0.02		0.11 ± 0.02
2 K	0.18 ± 0.12	0.19 ± 0.04	0.54 ± 0.03	0.09 ± 0.02
15 K	0.50 ± 0.08	0.85 ± 0.06	0.95 ± 0.02	0.05 ± 0.02

The remnant static contribution $y_0 S(\mathbf{Q}', 0)$ at 15 K is attributed to (spin-polarized) background magnetic scattering. Note that unpolarized background is suppressed in magnetic spin echo. In the ordered state ($T_N = 14.3$ K), the static signal is higher than this level; the most likely cause is Bragg peak contamination. The value of the static components at 50 mK and 2 K (using the "best fit" value) is the same within statistical error, suggesting that the scattering originates from the Bragg peak. Any significant dynamical scattering would have to occur on time scales >10 ns.

We therefore conclude that any quasielastic scattering with antiferromagnetic periodicity (as observed at 2 and 15 K) is insignificant deep inside the superconducting state; significant relaxation channels on time scales up to 10 ns are ruled out by the present results. These results are now examined within the context of the two principal models for the electronic structure.

The *itinerant* model assumes that all the $5f$ electrons are delocalized. Various Fermi-surface calculations [14–16] share the common feature of a closed surface intersected by the A-Γ axis ($a^* = 0$ in Fig. 3). In Refs. [14,16] this surface lies close to the Brillouin zone boundary. Figure 3(a) is a simplified sketch of some of the Fermi sheets described by Knöpfle *et al.* [14]. The "egg" surfaces appear to make a major contribution to the magnetic susceptibility as observed by TAS [17].

The superconducting energy gap has a wave vector dependent gap function with antiferromagnetic periodicity, $\Delta(\mathbf{k}) = -\Delta(\mathbf{k} + \mathbf{Q}_0)$ and even symmetry with respect to the antiferromagnetic Brillouin zone [7,16–19]. It is illustrated by a trapezoidal gap function in Fig. 3 [20]. This gives a fully gapped egg Fermi sheet at low temperatures, and is consistent with the absence of quasielastic scattering at 50 mK as observed in the present high resolution experiments. This is strong evidence that the egg surfaces are indeed dominant and that the "cigars," "cylinder," and (omitted) "party-hat" sheets, all of which carry low temperature nodes, do not contribute significantly to the quasiparticle magnetic susceptibility below T_{sc}.

The magnitude and form of the gap function (a sum of cosines) suggest that at higher temperatures (>1 K) the egg surfaces could be a source of quasielastic scattering around $\mathbf{Q}_0$ due to thermal quasiparticle excitations before passing through T_{sc}. This has indeed been observed by TAS [7]. The itinerant model, taken in combination with the gap, therefore offers an explanation of all of the key observations made in the neutron inelastic scattering studies.

The second model is a *dual* model. The $5f$ electron level is split into two subsystems: a localized $5f^2$ state and an

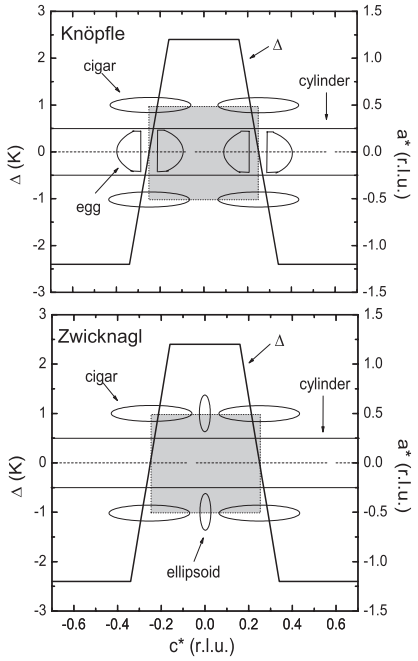

FIG. 3. The panels superpose, on a common c^* axis, an even parity energy gap function (left-hand ordinate) and schematics of (a) the itinerant model Fermi sheets [14] and (b) the dual model Fermi sheets [21]. In both cases, the party-hat sheet is omitted. The gray area marks the first Brillouin zone. Based on Fig. 4 from Ref. [17].

itinerant third $5f$ electron state. The Fermi surface for this configuration has been calculated by Zwicknagl *et al.* [21] and is illustrated in Fig. 3(b). There is no closed surface intersected by the A-Γ axis. The "ellipsoids" replace the "eggs," and for an even symmetry gap function, some of the arguments given above then apply to the ellipsoids. The key difference is that the ellipsoids will remain completely gapped until Δ collapses at T_{sc} in contradiction to previous neutron inelastic scattering data [7,22,23].

Moving now to the other part of the dual model, the localized $5f^2$ states are assumed to dominate the magnetic properties, which are described by a crystalline electric field (CEF) scheme. In the normal state both the quasielastic scattering at $\mathbf{Q}_0$ and the energy linewidth and dispersion of the 1.4 meV excitation are generated by level broadening via coupling with the itinerant states.

On passing below T_{sc}, the gap develops, condensing some of the itinerant quasiparticles. Within this model this might be assumed to sharpen the $5f^2$ levels, eliminating the $\mathbf{Q}_0$ quasielastic signal at low temperatures. However, the inelastic excitation at 1.4 meV remains broad and dispersive, and so the temperature independent relaxation rate seen below 7 K might be assumed to extend into the superconducting state. As no dynamics are seen in this experiment, the susceptibility must be zero. To reconcile this central experimental observation with the dual model within any simple interpretation, an unexpected modification of the localized $5f^2$ electron system would be required. To conclude, the Fermi-surface topology calculated within the itinerant model is entirely consistent with our findings.

In summary, this study shows that deep in the superconducting state UPd_2Al_3 shows no significant NSE scattering from low-energy modes existing over time scales ≤ 10 ns at 50 mK. Any nodes present at the Fermi surface do not contribute significant weight to the measured electronic susceptibility. These observations are related to the geometry of the gap function and the Fermi-surface topology. They place strong constraints on possible models for the origin and role of magnetic excitations in the unconventional superconductivity exhibited by this fascinating material, and we hope that the present results will stimulate further research.

We thank Noriaki Sato (Nagoya University, Japan) for providing the sample, and Oliver Stockert (MPI-CPfS Dresden, Germany), Peter Fouquet, and Bela Farago (ILL, France) for helpful discussions. E. B. would like to thank the European Commission for support in the frame of the TMR programme.

*Current address: Department of Physics, University of California, San Diego, 9500 Gilman Drive, La Jolla, CA 92093, USA.

[1] C. Geibel *et al.*, Z. Phys. B **84**, 1 (1991).
[2] A. Krimmel *et al.*, Z. Phys. B **86**, 161 (1992).
[3] M. Jourdan, M. Huth, and H. Adrian, Nature (London) **398**, 47 (1999).
[4] N. K. Sato *et al.*, Nature (London) **410**, 340 (2001).
[5] P. Thalmeier, Eur. Phys. J. B **27**, 29 (2002).
[6] N. Metoki, Y. Haga, Y. Koike, and Y. Onuki, Phys. Rev. Lett. **80**, 5417 (1998).
[7] N. Bernhoeft *et al.*, Phys. Rev. Lett. **81**, 4244 (1998).
[8] N. Metoki *et al.*, J. Phys. Soc. Jpn. **66**, 2560 (1997).
[9] F. Mezei, in *Neutron Spin Echo*, edited by F. Mezei (Springer-Verlag, Berlin, 1980), pp. 3–26.
[10] E. Blackburn, A. Hiess, M. C. Rheinstädter, N. Bernhoeft, and G. H. Lander (to be published).
[11] H. Kita *et al.*, J. Phys. Soc. Jpn. **63**, 726 (1994).
[12] L. Paolasini *et al.*, J. Phys. Condens. Matter **5**, 8905 (1993).
[13] E. Blackburn, Ph.D. thesis, Université Joseph-Fourier, Grenoble I, France, 2005.
[14] K. Knöpfle *et al.*, J. Phys. Condens. Matter **8**, 901 (1996).
[15] Y. Inada *et al.*, J. Phys. Soc. Jpn. **68**, 3643 (1999).
[16] P. M. Oppeneer and G. Varelogiannis, Phys. Rev. B **68**, 214512 (2003).
[17] N. Bernhoeft, Eur. Phys. J. B **13**, 685 (2000).
[18] J. Hessert *et al.*, Physica (Amsterdam) **230B–232B**, 373 (1997).
[19] T. Watanabe *et al.*, Phys. Rev. B **70**, 184502 (2004).
[20] A limited sum of cosines is the more likely form [16].
[21] G. Zwicknagl, A. Yaresko, and P. Fulde, Phys. Rev. B **68**, 052508 (2003).
[22] A. Hiess *et al.*, J. Phys. Condens. Matter **18**, R437 (2006).
[23] E. Blackburn *et al.*, Phys. Rev. B **74**, 024406 (2006).